UV Light-emitting Diode with Buried Polarization-induced n-AlGaN/InGaN/p-AlGaN Tunneling Junction

Yi Lu, Chuanju Wang, Victor Paiva De Oliveira, Zhiyuan Liu, and Xiaohang Li

Section S1: Band diagram and extracted potential barriers of four different III-nitride LED configurations

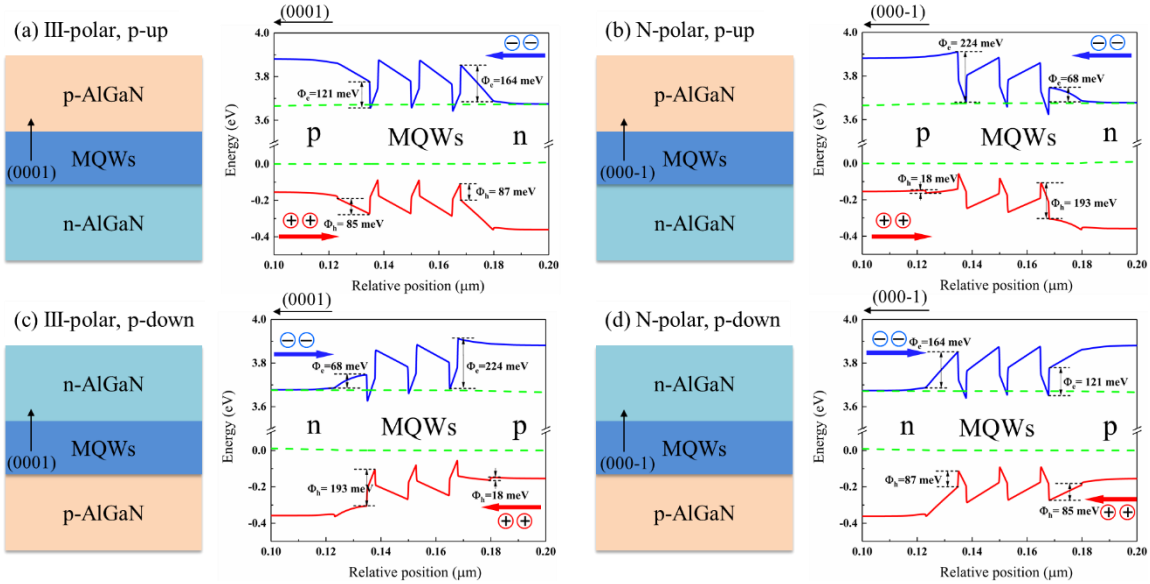

Fig. S1. The Schematic images of the four different III-nitride LED designs based on the combinations of III/N-polar and p-up/down. Along with the simulated band diagrams under forward bias. The four simulated LEDs all adopt three pairs $Al_{0.3}Ga_{0.7}N/Al_{0.2}Ga_{0.8}N$ MQWs.

Table SI. The extracted potential barrier heights for electron and holes injection or confinement from Fig. S1.

	Φe (injection) meV	Φe (confinement) meV	Φh (injection) meV	Φh (confinement) meV
(a) III-polar, p-up	164	121	85	87
(b) N-polar, p-up	68	224	18	193
(c) III-polar, p-down	68	224	18	193
(d) N-polar, p-down	164	121	85	87

Section S2: Schematic structure of BTJ LED and the layer details

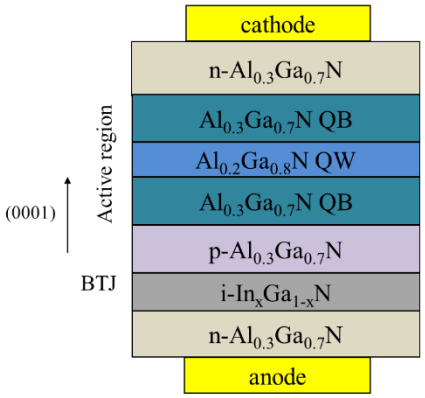

Layer	III% composition	Thickness (nm)	Doping (/cm^3)	
n-$Al_{0.3}Ga_{0.7}N$	0.3	60	5×10^{18}	
$Al_{0.3}Ga_{0.7}N$	0.3	12	1×10^{17}	×3 MQWs
$Al_{0.2}Ga_{0.8}N$	0.2	3	0	
$Al_{0.3}Ga_{0.7}N$	0.3	12	1×10^{17}	
p-$Al_{0.3}Ga_{0.7}N$	0.3	60	5×10^{19}	BTJ
i-$In_xGa_{1-x}N$	0~1	2~10	0	
n-$Al_{0.3}Ga_{0.7}N$	0.3	60	2.5×10^{20}	

Fig. S2. The structure of buried tunneling junction LED which could emit at ~320 nm and the layer details on the right table. Tunneling junction and active region are marked for the clarification.

The electrical properties of BTJ LEDs are investigated by simulating the UV LED with different In% and InGaN thicknesses. The direct metal contact between the anode and the bottom n-AlGaN is to focus on the investigation of the vertical electrical field and current injection without worrying about the current spreading issue in planar LED. Moreover, this freestanding n-AlGaN template could also be realized by the laser liftoff [1] or electrochemical etching [2].

For the LED simulation, Advanced Physical Models of Semiconductor Devices (APSYS) developed by Crosslight Inc. was employed [3]. The built-in interface charges induced by spontaneous and piezoelectric polarization were based on [4]. The 6 × 6 k·p model developed by Chuang [5] and Chang [6] was adopted for calculating the band structures. The interface charge densities were assumed to be 50% of total charges considering the defects of layers and the charge densities screened by injected carriers under bias were calculated self-consistently. The activation energy of acceptor in p-type AlGaN was set based on the experimental data measured by Kinoshita et al [7] . We set the Shockley-Read-Hall (SRH) recombination lifetime, the Auger recombination coefficient, radiative recombination coefficient and light extraction efficiency as 15 ns, 2.88×10^{-30} cm^6/s, 2.13×10^{-17} cm^3/s, and 10% respectively [8]. The bandgap bowing factor of AlGaN was set as 0.94, and the band offset ratio of AlGaN and InGaN materials was decided to 0.67/0.33 [9]. Effective mass parameters were set according to the data in [10] . The p-AlGaN has ~1% activation ratio with 310 meV activation energy [11].”

Section S3: Polarization-induced tunneling details

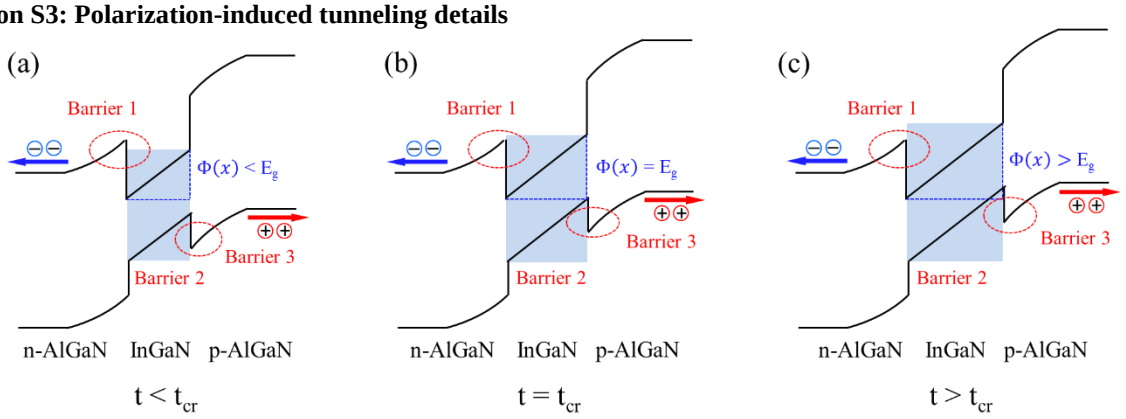

Fig. S3. The Schematic of polarization-induced tunneling when InGaN thickness t (a) t< t_{cr}, (b) t= t_{cr}, (c) t> t_{cr}.

Fig. S3 (a)-(c) are the schematics of the tunneling probability when the InGaN thickness is less, equal, or larger than the t_{cr}. Barrier 1 and 3 are the depletion regions resulting from the doping in AlGaN and the band offset between AlGaN and InGaN. Barrier 2 comes from the InGaN thickness as well as the E_c-E_v overlap. When t= t_{cr}, the build-in potential $\Phi(x)$ is equal to the bandgap (E_g) of InGaN. While t< t_{cr} or t> t_{cr}, the potential is less than or more than the E_g of InGaN, respectively.

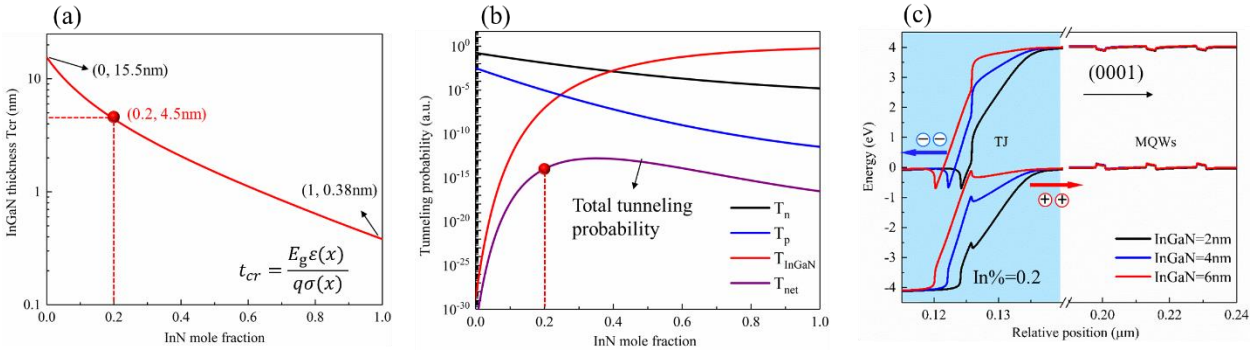

Fig. S4. (a) Critical thickness t_{cr} versus In%, (b) tunneling probability T_n, T_p, T_{InGaN}, T_{net} versus In%, (c) band diagram of the BTJ LEDs with 2, 4, and 6 nm $In_{0.2}Ga_{0.8}N$ tunneling layers under bias, the blue region describes the BTJ area.

Fig. S4 (a) shows the t_{cr} versus the In% according to $t_{cr} = \frac{E_g \varepsilon(x)}{q\sigma(x)}$. For In% from 0 to 1, the corresponding t_{cr} reduces from 15.5 nm to 0.38 nm. For Fig. S4 (b), T_n and T_p decrease with the increase of In% due to that the depletion region widths become wider when ΔE_c and ΔE_v enlarge. Meanwhile, T_{InGaN} keeps increasing due to that the enlarged polarization charge leads to the reducing of t_{cr}, making the interband tunneling happens within a narrow region. Consequently, the T_{net} has a peak value at In% =~0.3. Fig. S4 (c) shows the energy band diagrams of BTJ UV LEDs with 2, 4, and 6 nm InGaN tunneling layer under forward bias.

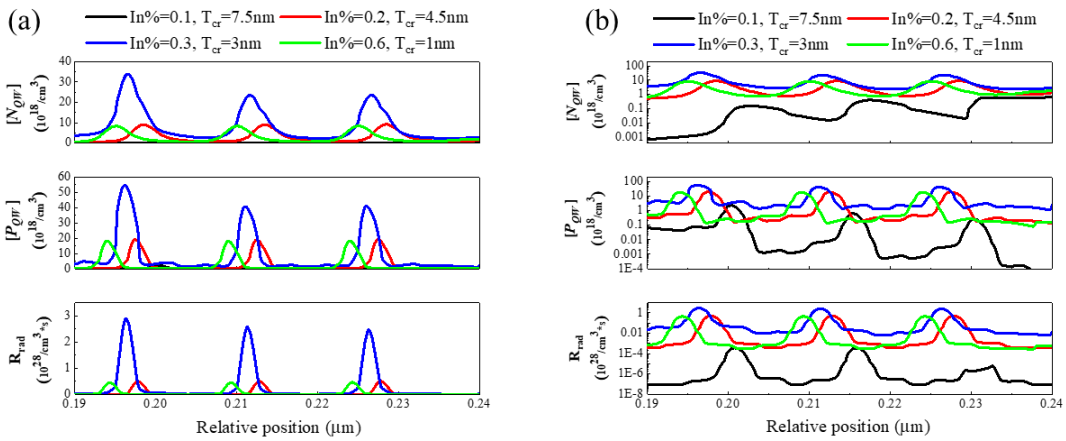

Fig. S5. [N_{QW}], [P_{QW}], and [R_{rad}] distribution in the QWs for different In% and InGaN thicknesses with (a) linear scale and (b) logarithmic scale.

Fig. S5 (a) (b) show the [N_{QW}], [P_{QW}], and [R_{rad}] distribution in the QWs for different In% and InGaN thicknesses. The combination of In%=0.3 and T_{cr}=3 nm with the highest tunneling probability shows the highest carrier concentration and thus highest R_{rad}. The increase of R_{rad} is from the increase of both electron and hole concentrations in the QWs.

Table SII. The polarization charge difference between $Al_{0.3}Ga_{0.7}N/In_yGa_{1-y}N$ with different In composition.

$Al_xGa_{1-x}N$	0.3	0.3	0.3	0.3	0.3	0.3	0.3
$In_yGa_{1-y}N$	0	0.05	0.1	0.15	0.2	0.25	0.3
$\Delta p(C/m^2)$	0.0362	0.0424	0.0493	0.057	0.0655	0.0747	0.0846

Table SII shows that the polarization charge difference between $Al_{0.3}Ga_{0.7}N/In_xGa_{1-x}N$ interface increases with the In% (y) in $In_yGa_{1-y}N$, resulting in the decrease of t_{cr} from 15.5 nm to 0.38 nm in Fig. S4 (a).

Table SIII. In% in InGaN and corresponding critical thickness (t_{cr}), tunneling probability, spontaneous emission rate (R_{sp}), and output power density.

In%	T_{cr} (nm)	Tunneling probability (a.u.)	R_{sp} (a.u.)	Power density (W cm^{-2})
0.1	7.5	1.431×10^{-18}	2.8	0.05
0.2	4.5	1.59×10^{-14}	4113	112
0.3	3	1.280×10^{-13}	15720	656
0.6	1	1.214×10^{-14}	3896	101

References:

[1] C.-F. Chu *et al.*, "Study of GaN light-emitting diodes fabricated by laser lift-off technique," *J. Appl. Phys.*, vol. 95, no. 8, pp. 3916-3922, 2004.

[2] J. Park, K. M. Song, S.-R. Jeon, J. H. Baek, and S.-W. Ryu, "Doping selective lateral electrochemical etching of GaN for chemical lift-off," *Appl. Phys. Lett.*, vol. 94, no. 22, p. 221907, 2009.

[3] A. Version, "by Crosslight Software Inc., Burnaby, Canada," ed.

[4] V. Fiorentini, F. Bernardini, and O. Ambacher, "Evidence for nonlinear macroscopic polarization in III–V nitride alloy heterostructures," *Appl. Phys. Lett.*, vol. 80, no. 7, pp. 1204-1206, 2002.

[5] S. Chuang and C. Chang, "k· p method for strained wurtzite semiconductors," *Phys. Rev. B*, vol. 54, no. 4, p. 2491, 1996.

[6] S. Chuang and C. Chang, "A band-structure model of strained quantum-well wurtzite semiconductors," *Semicond. Sci. Technol.,* vol. 12, no. 3, p. 252, 1997.
[7] T. Kinoshita, T. Obata, H. Yanagi, and S.-i. Inoue, "High p-type conduction in high-Al content Mg-doped AlGaN," *Appl. Phys. Lett.,* vol. 102, no. 1, p. 012105, 2013.
[8] J. Yun, J.-I. Shim, and H. Hirayama, "Analysis of efficiency droop in 280-nm AlGaN multiple-quantum-well light-emitting diodes based on carrier rate equation," *Appl. Phys. Express,* vol. 8, no. 2, p. 022104, 2015.
[9] C. Coughlan, S. Schulz, M. A. Caro, and E. P. O'Reilly, "Band gap bowing and optical polarization switching in Al Ga N alloys," *Phys. Status Solidi,* vol. 252, no. 5, pp. 879-884, 2015.
[10] A. Punya and W. R. Lambrecht, "Valence band effective-mass Hamiltonians for the group-III nitrides from quasiparticle self-consistent G W band structures," *Phys. Rev. B,* vol. 85, no. 19, p. 195147, 2012.
[11] J. Li, T. Oder, M. Nakarmi, J. Lin, and H. Jiang, "Optical and electrical properties of Mg-doped p-type AlxGa1− xN," *Appl. Phys. Lett.,* vol. 80, no. 7, pp. 1210-1212, 2002.